ECS Journal of Solid State Science and Technology, **6** (2) Q3012-Q3021 (2017)
2162-8769/2017/6(2)/Q3012/10/$33.00 © The Electrochemical Society

JSS Focus Issue on Ultrawide Bandgap Materials and Devices

Review—Hexagonal Boron Nitride Epilayers: Growth, Optical Properties and Device Applications

H. X. Jiang[z] and J. Y. Lin[z]

Department of Electrical and Computer Engineering, Texas Tech University, Lubbock, Texas 79409, USA

This paper provides a brief overview on recent advances made in authors' laboratory in epitaxial growth and optical studies of hexagonal boron nitride (*h*-BN) epilayers and heterostructures. Photoluminescence spectroscopy has been employed to probe the optical properties of *h*-BN. It was observed that the near band edge emission of *h*-BN is unusually high and is more than two orders of magnitude higher than that of high quality AlN epilayers. It was shown that the unique quasi-2D nature induced by the layered structure of *h*-BN results in high optical absorption and emission. The impurity related and near band-edge transitions in *h*-BN epilayers were probed for materials synthesized under varying ammonia flow rates. Our results have identified that the most dominant impurities and deep level defects in *h*-BN epilayers are related to nitrogen vacancies. By growing *h*-BN under high ammonia flow rates, nitrogen vacancy related defects can be eliminated and epilayers exhibiting pure free exciton emission have been obtained. Deep UV and thermal neutron detectors based on *h*-BN epilayers were shown to possess unique features. It is our belief that *h*-BN will lead to many potential applications from deep UV emitters and detectors, radiation detectors, to novel 2D photonic and electronic devices.

Manuscript received July 27, 2016. Published September 7, 2016. This was Paper 1211 from the San Diego, California, Meeting of the Society, May 29- June 2, 2016. *This paper is part of the JSS Focus Issue on Ultrawide Bandgap Materials and Devices.*

As a member of the III-nitride wide bandgap semiconductor family, boron nitride (BN) has received much less attention in comparison with other nitride semiconductors. Due to its extraordinary physical properties,[1–11] such as high chemical stability, thermal conductivity, melting temperature, electrical resistivity, bandgap ($E_g \sim 6.5$ eV), optical absorption near the band edge ($\sim 7.5 \times 10^5$/cm), negative electron affinity, and thermal neutron capture cross-section, BN appears to be the material of choice for emerging applications, including deep UV (DUV) optoelectronics, electron emitters and neutron detectors. Although, BN exists in various crystalline forms, the hexagonal form is isostructural to graphite and is the stable phase of BN synthesized at any temperature and under normal pressure.[1–9] Due to its close lattice match to graphite and its chemical inertness and resistance to oxidation, hexagonal boron nitride (*h*-BN) is considered an ideal template and barrier material for the construction of two-dimensional (2D) heterostructures and quantum wells.[12–17] Similar to graphene, *h*-BN is expected to possess rich new physics due to its layered structure with the exception that it is also complementary to graphene because of its wide bandgap.

BN has been well known both as an excellent electrical insulator and thermal conductor. In recent years, lasing action in the DUV region (~225 nm) by electron beam excitation was demonstrated in small *h*-BN bulk crystals synthesized by a high pressure/temperature technique,[18] raising its promise as a semiconductor for realizing chip-scale DUV light sources/sensors. So far, *h*-BN bulk crystals with sizes up to millimeters can be grown. Other than small size, bulk crystal growth has disadvantages of difficulty to control growth conditions such as intentional doping and formation of device structures and is most suitable for producing substrates if a relative large size can be realized. Until now, research on layer structured materials is mostly based on manually exfoliating individual layers from layer-structured crystals and manually stacking them to form 2D heterostructures. This has been useful for the study of new physics, but prohibits the realization of wafer-scale processing, QW design, and doping processes, which are prerequisites for practical device implementation. The ability for synthesizing wafer-scale semiconducting *h*-BN epitaxial layers with high crystalline quality and electrical conductivity control is highly desirable for fundamental understanding as well as for the exploration of emerging applications of this interesting material system.

[z]E-mail: hx.jiang@ttu.edu; jingyu.lin@ttu.edu

By leveraging advances and prior knowledge in AlN epi-growth, we have demonstrated the growth of wafer scale *h*-BN epilayers on sapphire, AlN/sapphire template, and SiC substrates by metal organic chemical vapor deposition (MOCVD). MOCVD is a proven technique with the ability to precisely and reproducibly deposit very thin layers (single atomic layers) to thick epilayers (tens of μm in thickness). This paper summarizes recent progress made primarily in authors' laboratory on synthesizing *h*-BN epilayers by MOCVD and studies of their structural and optoelectronic properties. Detailed comparison studies with high quality and well characterized AlN epilayers have been carried out to reveal the unique two-dimensional (2D) nature of *h*-BN. Deep UV emitters and detectors and thermal neutron radiation detectors based *h*-BN have been fabricated and the results represent a major step toward the realization of *h*-BN based practical devices.

MOCVD Growth and Structural Properties

Hexagonal BN epitaxial layers were synthesized by MOCVD using triethylboron (TEB) source and ammonia (NH_3) as B and N precursors, respectively.[19,20] Prior to epilayer growth, a 20 nm BN buffer layer was first deposited on sapphire substrate at 800°C. The typical *h*-BN epilayer growth temperature was about 1300°C using hydrogen as a carrier gas. For *h*-BN epilayer growth, the parasitic reaction between triethylborane (TEB) and NH_3 in the gas phase is a problem which resembles the reaction between NH_3 and TMAl during AlN epilayer growth.[19–24] The surface migration of boron atoms is poor because the B-N bond is strong and parasitic reaction between TEB and NH_3 is severe. The by-products of the pre-reaction deposited on the wafer cause a rough surface and high crystalline defect density. Modulation pulsed growth with alternating supplies of group III (TEB) and group V (NH_3) precursors can significantly suppress the parasitic reactions in the gas phase.[21–23] In the modulation pulsed growth process, there are 4 basic parameters that need to be optimized: "on" time for NH_3 flow (t_{on}^{NH3}), "on" time for TEB flow (t_{on}^{TEB}), TEB flow rate (R_{TEB}), and NH_3 flow rate (R_{NH3}). These parameters can be varied independently to produce materials with improved crystalline quality. The pulse sequence can also be varied to achieve different growth rates.

X-ray diffraction (XRD) θ-2θ scan of *h*-BN shown in Fig. 1a revealed a *c*-lattice constant ~6.67 Å, which closely matches to the bulk *c*-lattice constant of *h*-BN (c = 6.66 Å),[1–4] affirming that our MOCVD grown BN films are of single hexagonal phase. Secondary ion mass spectrometry (SIMS) results shown in Fig. 1b indicated

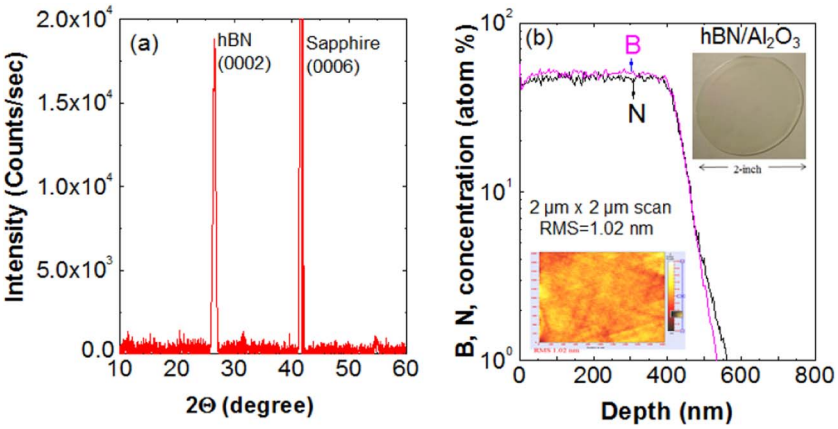

Figure 1. (a) XRD θ-2θ scan of a 1 μm thick *h*-BN epilayer deposited on sapphire; (b) SIMS data obtained for a 0.5 μm thick *h*-BN epilayer. The insets show an AFM image of *h*-BN epilayer over a 2 × 2 μm^2 area scan and an optical image of a 2-inch wafer of *h*-BN epilayer (after Refs. 19 & 20).

that *h*-BN epilayers have excellent stoichiometry. As shown in the inset of Fig. 1b, thin *h*-BN epilayers (<1 μm) exhibit good surface morphologies and RMS values around 1 nm can be obtained. However, the surface morphology of *h*-BN epilayers becomes poorer with an increase in the *h*-BN layer thickness and requires further improvement.

Figure 2 compares XRD characterization results for AlN and *h*-BN. It can be seen that the XRD intensity of the (0002) peak of *h*-BN is about 30 times lower than that of AlN epilayer with the same thickness.[25] As shown in Fig. 2b, the XRD rocking curve of the (0002) diffraction peak has a full width at half maximum (FWHM) of ∼380 arcsec for the *h*-BN,which is comparable to those of typical high quality GaN epilayers deposited on sapphire.[26] This is a dramatic improvement over previously reported values for *h*-BN films (1.5°–0.7°),[27] but is much broader than the typical FWHM of high quality AlN epilayers of <60 arcsec.[25] These results signify that it is feasible to obtain *h*-BN epilayers with high crystalline quality by MOCVD and that the epitaxial layers of *h*-BN is still in its early stage of development.

Optical Properties

Origin of high emission efficiency.—Though optical properties of the band edge transitions in *h*-BN have been studied and reported in the last 10 years, mostly from *h*-BN bulk crystals, many fundamental properties remain unknown. What we know today about the optical properties of *h*-BN can be summarized below:

(a) *Ultra-high bandgap* - Both theoretical and experimental results indicate that the bandgap of *h*-BN is around 6.5 eV.[28-30]
(b) *High optical emission and absorption* - The previously measured optical absorption is as high as 7.5 × 10^5/cm.[7]
(c) *Very large exciton energy* – The exciton binding energies is about 0.7 eV in *h*-BN bulk crystals and 2.1 eV in *h*-BN monolayers).[28–31]

As shown in Figs. 3a and 3b, the photoluminescence (PL) emission intensity of the band edge transition in *h*-BN is more than 2 orders of magnitude higher than that of AlN when the two samples are measured side by side for a direct comparison. Notice that the 10 K spectrum of *h*-BN is multiplied by a factor of 1/500, while the 300 K spectrum is multiplied by a factor of 1/100.[31,32] The results imply that *h*-BN based DUV devices potentially could be even more efficient than AlN.

The results shown in Fig. 3 also inferred a very large oscillator strength and high density of states near the band edge. Our recent work has shown that the strong optical transitions in *h*-BN partly originates from the unusually strong $p \rightarrow p$-like transitions due to its quasi-2D nature, giving rise to very high density of states near the band edge.[31] It is interesting to note that *h*-BN is the only quasi-2D inorganic semiconductor with such a large energy bandgap. In addition, the layer structured *h*-BN provides a natural 2D system which can result in an increase in the exciton binding energy and oscillator strength over the 3D systems such as AlN.[28–32] Another factor that accounts for this efficient band-edge emission in *h*-BN is the high band-edge optical absorption coefficient.[7,24]

The previously measured band-edge optical absorption coefficient (α) of *h*-BN is unusually high (∼7.5 × 10^5 cm^{-1})[7] and is more than 3 times higher than that of AlN (∼2 × 10^5 cm^{-1}).[33] This high optical absorption property can be understood by writing the optical absorption (I) as,[24]

$$I = I_0(1 - e^{-t/\lambda}); \quad [1]$$

where λ is the optical absorption length. On the other hand, we can rewrite Eq. 1 as follows,

$$I/I_0 \approx (t/\lambda), \text{ for}(t/\lambda) \ll 1; \quad [2]$$

One important features of graphene is that its absorption is $\pi e^2/\hbar c = \pi\alpha = 2.3\%$, where $\alpha = e^2/\hbar c$ is the fine structure constant, which describes the coupling between light and relativistic electrons.[34] If we

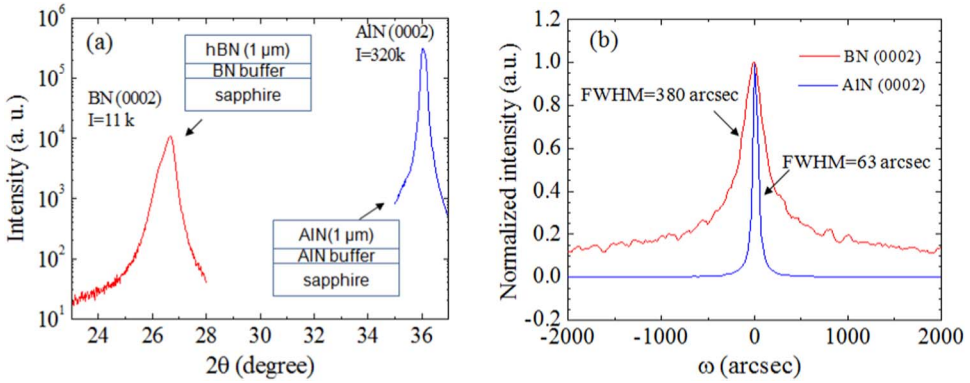

Figure 2. Comparison XRD results of *h*-BN and AlN epilayers: (a) θ-2θ scans and (b) rocking curves of the (0002) diffraction peaks.

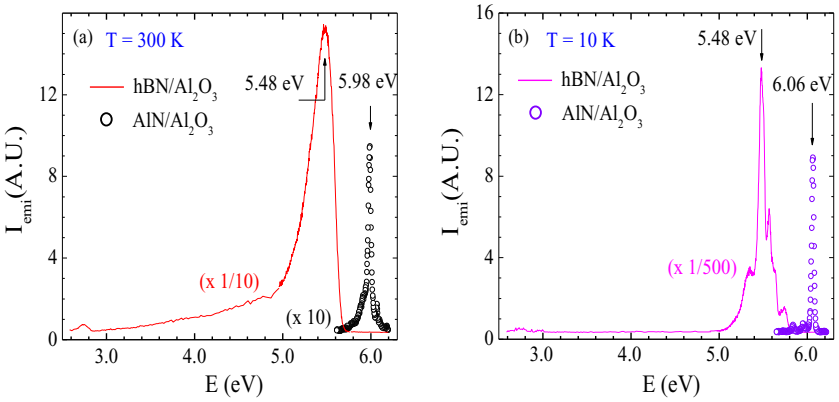

Figure 3. Comparison DUV PL spectra of *h*-BN and AlN epilayers measured at (a) 10 K and (b) 300 K (after Refs. 31 and 32).

assume the same holds for the above bandgap optical absorption in *h*-BN, we then have the optical absorption of *h*-BN = 2.3% per layer (3.33 Å). This means that $I/I_0 = (t/\lambda) = 0.023$ with t = 3.33 Å. This gives,

$$\lambda = t/0.023 = 3.33\,\text{Å}/0.023 = 144.8\,\text{Å}$$

$$\alpha = 1/\lambda = 1/144.8\,\text{Å} = 6.9 \times 10^{-3}/\text{Å} \approx 7 \times 10^5/\text{cm}.$$

This estimated value of 7×10^5/cm for the band-edge optical absorption coefficient based on the optical absorption concept of graphene agrees exceptionally well with the previously measured value of about 7.5×10^5/cm.[7] This means that only a very thin layer of *h*-BN with approximately 70 nm (~5λ) in thickness will absorb all incoming above bandgap photons. This together with its inherent nature of layered structure makes *h*-BN an exceptionally efficient emitter.

Moreover, electron–hole pairs in *h*-BN form very tightly bound excitons with a huge exciton binding energy ($E_x \sim 0.74$ eV) or small Bohr radius ($a_B \sim 8$ Å) due to its low dielectric constant and layered structure.[28–31] E_x is at least one order of magnitude larger than those in any other inorganic semiconductors (the reported E_x for AlN ranges from 60 – 80 meV[35–37]). The consequences of this large E_x value on the optical transitions in *h*-BN are not yet fully explored; the oscillator strength of small Bohr radius exciton can be very huge (on the order of unity) due to the strong overlapping between electron and hole wavefunctions, supporting high emission efficiency of *h*-BN.

TE emission.—Figure 4a compares the polarization-resolved band-edge PL emission spectra of *h*-BN and AlN epilayers measured at 10 K.[31] The PL emission spectral line shape for *h*-BN shown in Fig. 4a for the configuration with emission polarization along the crystal c-axis (E_{emi}//c) is observed to be very similar to that in the ($E_{emi} \perp c$) configuration. However, the emission intensity is about 1.7 times stronger in ($E_{emi} \perp c$) configuration, which is in sharp contrast to the polarization-resolved PL spectra of AlN shown in Fig. 4b.[38] However, the emission polarization of *h*-BN is similar to GaN.[38,39] As shown in Fig. 4b, the band-edge emission in $Al_xGa_{1-x}N$ evolves from $E_{emi} \perp c$ in GaN to E_{emi}//c in AlN. It is now a well-established fact that the band-edge emission in AlN is polarized along the c-axis, (E_{emi}//c), due to the nature of its band structure (the negative crystal-field splitting in AlN).[39] This polarization property of AlN has a profound impact on the device applications. For instance, for UV light emitting diodes (LEDs) using c-plane Al-rich $Al_xGa_{1-x}N$ as active layers, the most dominant emission will be polarized along the c-axis (E_{emi}//c), which implies that UV photons can no longer be extracted easily from the surface.[38] Thus, incorporating methods such as photonic crystals for enhancing the light extraction is critical in AlGaN UV LEDs.[40] Furthermore, in contrast to all conventional semiconductor laser diodes with lasing output polarized in the transverse-electric

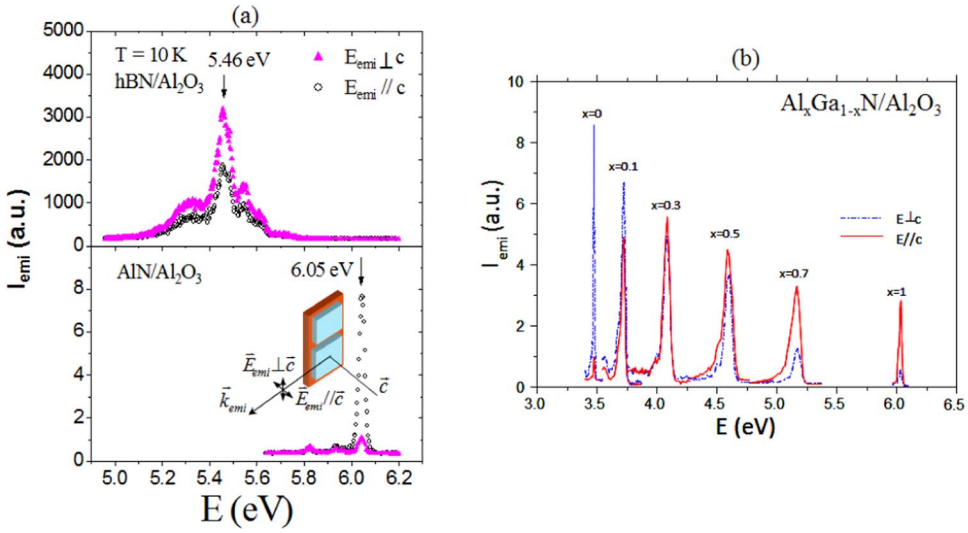

Figure 4. (a) Comparison of polarization-resolved low temperature (10 K) band-edge PL spectra of *h*-BN and AlN epilayer with emission polarization parallel (E_{emi}//c) and perpendicular ($E_{emi} \perp c$) to the c-axis. Excitation laser line is polarized in the direction perpendicular to the c-axis (E_{emi}//c) [after Ref. 31]. (b) Polarization-resolved low temperature (10 K) band-edge PL spectra of $Al_xGa_{1-x}N$ showing that the polarization switches from $E_{emi} \perp c$ in GaN to E_{emi}//c to AlN (after Ref. 39).

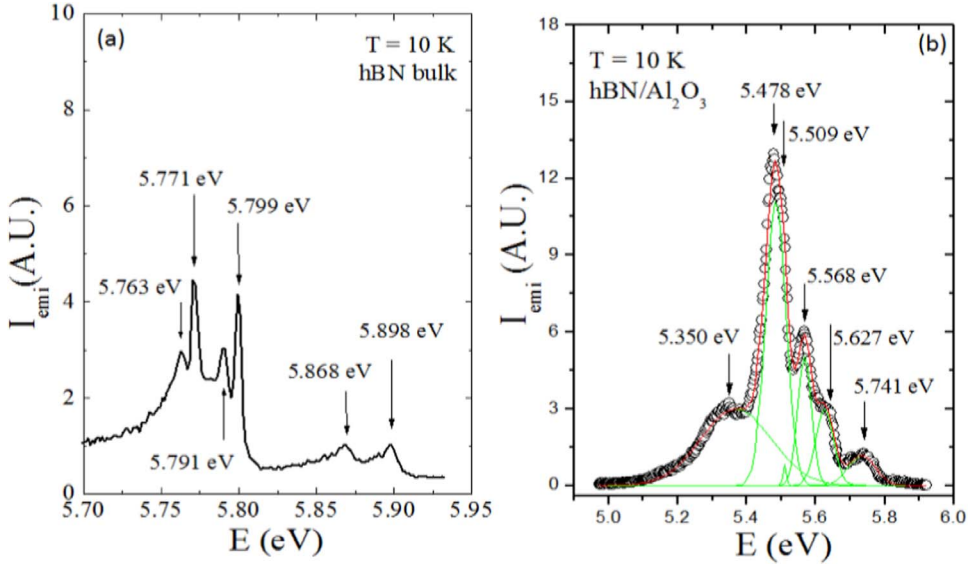

Figure 5. Comparison of PL spectra between an (a) *h*-BN bulk crystal and (b) epilayer (after Refs. 30 & 32).

field (TE) mode, it was predicated[38] and experimentally verified[41] that lasing radiation from c-plane Al-rich $Al_xGa_{1-x}N$ based laser diodes is strongly polarized in the transverse-magnetic-field (TM) mode. These are currently critical issues facing the development of deep UV light emitting devices based on AlGaN. Thus, the observed predominant ($E_{emi} \perp c$) polarization of the band-edge emission in *h*-BN is an advantageous feature over AlN for UV light emitting device applications.

***Nature of deep-level impurities in* h-*BN*.—**As indicated by the comparison XRD results between *h*-BN and AlN shown in Figs. 2a and 2b, much improvements in crystalline quality of *h*-BN epilayer are still needed. On the other hand, the basic properties of *h*-BN epilayers can also be calibrated against those of *h*-BN bulk crystals, despite the fact that *h*-BN bulk crystals are still small in size and contain multi-domains. Consequently, XRD rocking curves cannot be measured for *h*-BN bulk crystals. However, individual *h*-BN bulk crystallites possess excellent optical properties. In Fig. 5, we present the comparison of low temperature (10 K) band-edge PL emission spectrum of an *h*-BN bulk crystal with that of an *h*-BN epilayer. It can be seen that the fine features in the spectral region from 5.70 to 5.95 eV in the *h*-BN bulk crystal are clearly resolved, but absent in the *h*-BN epilayer. The four main emission peaks located at 5.771, 5.799, 5.868, and 5.898 eV can be attributed to four excitonic transitions.[28,30,42] The main PL emission peak around 5.5 eV observed in *h*-BN epilayer are related to impurity bound exciton transitions.

A comprehensive study on the impurity properties of *h*-BN for materials produced under controlled growth conditions is needed to provide input for approaches toward the improvement of material quality and elimination of undesired defects. We have investigated *h*-BN epilayers grown by MOCVD under different NH_3 flow rates to allow the studies via PL of the roles of nitrogen vacancy (V_N) in *h*-BN. Figure 6a shows the room temperature PL spectra of *h*-BN epilayers grown under varying NH_3 flow rates ranging from 0.2 to 1.5 SLM,[43] whereas Fig. 6b shows the low temperature (T = 10 K) PL spectra of *h*-BN epilayers grown under varying NH_3 flow rates ranging from 0.3 to 20 SLM with all other growth conditions being identical.[44] The samples were placed side-by-side during the PL spectra measurements for spectral feature and emission intensity comparison. The results shown in Fig. 6a reveal three impurity peaks below 5 eV which are related to a donor-acceptor pair (DAP) transition (zero-phonon emission line at 4.12 eV and its phonon replicas at 3.92 and 3.72 eV).[45–47] As shown in Fig. 6b, in the samples grown under low NH_3 flow rates (between 0.3 up to 1.0 SLM), two other emission lines around 5.3 eV and 5.5 eV are also clearly resolvable, corresponding to the *q*-DAP transition and bound exciton transition, respectively.[32,42,48–51]

It is clear that the emission intensities of impurity related transition lines (DAP, q-DAP, and bound exciton transitions) all decrease continuously with an increase of the NH_3 flow rate. The most remarkable feature revealed in Fig. 6b is that the impurity related emission lines disappear altogether and a sharp free exciton emission line emerges at 5.735 eV when the NH_3 flow rate is increased to above 16 SLM. The complete elimination of the impurity emission line in *h*-BN epilayers grown under high NH_3 rates clearly speaks for the fact that these emission lines are related to V_N or impurities related to V_N. The results demonstrate that it is possible to completely eliminate V_N and its associated defects in *h*-BN epilayers by employing nitrogen-rich growth conditions. The free exciton emission line has been observed for the first time in *h*-BN epilayers. During the growth of *h*-BN epilayers, NH_3 serves as the source of the nitrogen atoms. The calculated formation energy of V_N in *h*-BN is quite low.[52] V_N and carbon impurities occupying the nitrogen sites (C_N) are known to be two of the most common impurities in *h*-BN.[53–59] The energy peak position of the exciton transition in *h*-BN epilayers shown in Fig. 6b is lower than those in *h*-BN bulk crystals shown in Fig. 5a, possibly attributed to different symmetry breaking mechanisms, strains, and material imperfections in epilayers versus in bulk crystals.

As shown in Fig. 7a, temperature-dependent emission intensity of the 4.1 eV line was measured from 10 K to 800 K, which provided an activation energy of ~0.1 eV for the shallow impurity involved in the DAP transition. Using a bandgap value of 6.5 eV,[28–31,60,61] we deduced the energy level of the deep impurity level involved in the DAP transition to be $E_g - E_{shallow} - h\nu_{emi} = 6.5$ eV- 0.1 eV – 4.1 eV = 2.3 eV by neglecting the coulomb interaction between ionized donors and acceptors. The measured energy levels together with previous theoretical insights on the formation energies of the impurities and defects in *h*-BN suggest that V_N and carbon impurities occupying the nitrogen sites (C_N), respectively, are the most probable shallow donor and deep acceptor impurities involved in the DAP transition at 4.1 eV.

Moreover, the results shown in Fig. 7b infer that the *q*-DAP emission line near 5.3 eV also involves V_N shallow donor. The energy level of the involved deep impurity can also be deduced from $E_g - E_{shallow} - h\nu_{emi} = 6.5$ eV- 0.1 eV – 5.3 eV = 1.1 eV. In obtaining this energy level, $E_g = 6.5$ eV is used and the coulomb interaction between ionized donors and acceptors has been neglected. With the known presence of a deep level impurity with an activation energy of about 1.1 eV, it should be possible to observe a band-to-impurity type transition by measuring the PL emission spectra in the near infrared

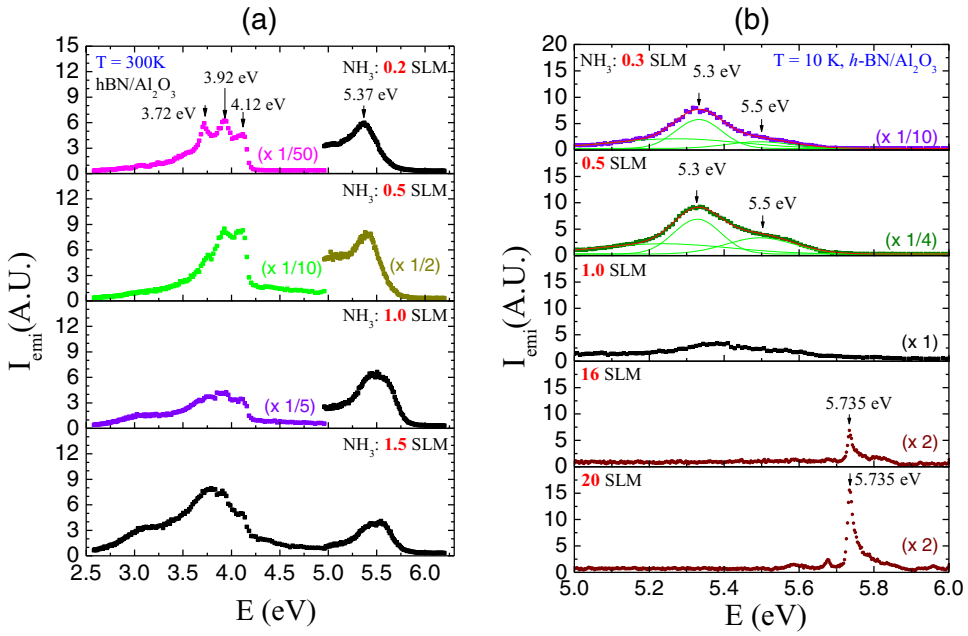

Figure 6. (a) 300 K PL spectra of impurity related transitions in *h*-BN epilayers grown at 1350°C under different NH_3 flow rates (R_{NH_3}). (b) 10 K PL spectra of near band-edge transitions in *h*-BN epilayers grown under different NH_3 flow rates. The spectra are vertically shifted to provide a clearer presentation (after Refs. 43 and 44).

region near 1.1 eV. This is indeed the case. As shown in Fig. 7b, a rather broad weak emission line with its peak energy around 1.2 eV was observed in the *h*-BN epilayer grown under an NH_3 flow rate of 1.5 SLM. This emission peak is most likely corresponding to a band-to-impurity transition between the deep acceptor involved in the *q*-DAP transition and the valence band. Previous theoretical studies have indicated that a substitutional carbon impurity on a nitrogen site could induce two deep defect levels localized on the carbon atom.[53,59]

The complete elimination of the 5.5 eV emission line in materials grown under high NH_3 rates points to the fact that the 5.5 eV emission line is related to the recombination of an exciton bound to V_N or to an impurity occupying the nitrogen site. Based on the energy peak position of the free exciton emission line observed in *h*-BN epilayers at 5.735 eV, the binding energy of the bound exciton (E_{BX}) related to the 5.5 eV emission line can be estimated to be around 0.24 eV. According to Haynes' rule, the binding energy of a bound exciton is about 10% of the impurity binding energy, neglecting the central cell correction. This infers that the energy level of the impurity involved in the bound exciton transition at 5.5 eV is around 2.4 eV, which is very close to the value of 2.3 eV for the energy level deduced for C_N involved in the DAP transition near 4.1 eV. Therefore, it is highly plausible that the 5.5 eV emission line is due to the recombination of excitons bound to C_N deep acceptors (A^0,X), or I_1 type transition. We speculate that carbon impurities originate from the boron precursor (TEB source). An interesting point that is worth mentioning is that the I_1 transition (excitons bound to acceptors) is more readily observable than the I_2 type transition (excitons bound to donors) in *h*-BN epilayers, whereas in all other III-nitride semiconductors (AlN, GaN, InN) the I_2 type transition is more probable. This is due to the fact that the Fermi level in undoped *h*-BN lies below the middle of the energy gap and undoped *h*-BN materials tend to be slightly p-type, while undoped AlN, GaN, and InN tend to be n-type. In this sense, *h*-BN is more like diamond than other III-nitride semiconductors.

Based on the understanding presented above, the emission lines related to V_N at 4.1, 5.3 and 5.5 eV can be minimized or completely eliminated by employing high NH_3 flow rates during the *h*-BN epilayer growth. With the determination of the energy levels involved, we have constructed the energy diagrams illustrating the optical processes of the observed impurity transition lines in *h*-BN epilayers, as depicted in Fig. 8a and bound exciton transition in Fig. 8b. These results provide

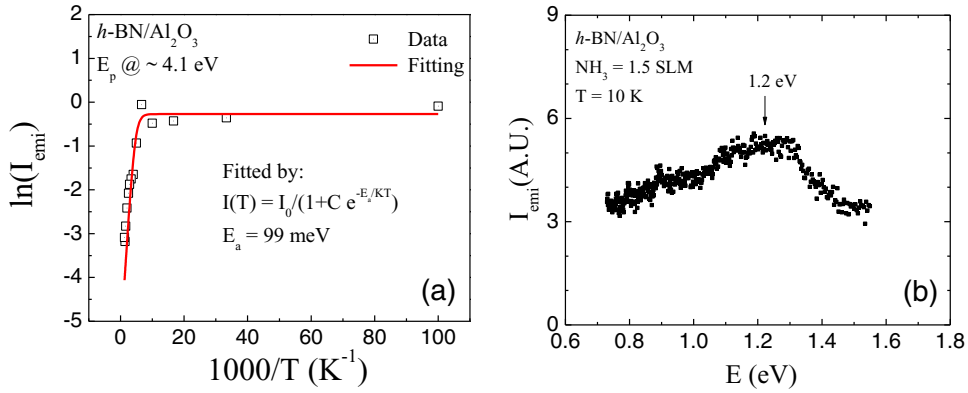

Figure 7. (a) Arrhenius plot of integrated PL emission intensity of the DAP transition near 4.1 eV on an *h*-BN epilayer grown under 1.5 SLM NH_3 flow rate. (b) PL spectrum of an *h*-BN epilayer grown at an NH_3 flow rate of 1.5 SLM measured in the near infrared spectral region exhibiting an emission line at 1.2 eV (after Refs. 43 and 44).

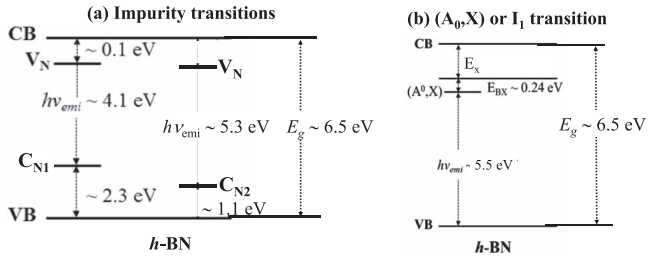

Figure 8. (a) Energy diagram illustrating the optical processes of the widely observed impurity emission lines near 4.1 eV and 5.3 eV in *h*-BN. (b) Energy diagram illustrating the optical process of the widely observed bound exciton emission line near 5.5 eV in h-BN.

an improved understanding of V_N related impurities/defects as well as their effects on the optical and doping properties of *h*-BN epilayers. Our results also demonstrate that by monitoring the impurity related PL emission peaks in *h*-BN while varying the growth conditions, it is possible to obtained epilayers with reduced defect densities.

P- and n-type Doping in *h*-BN

In sharp contrast to other members of the III-nitride family, p-type *h*-BN seems more readily obtained than n-type, similar to the case in diamond. We have shown that it is possible to convert *h*-BN to p-type by Mg doping.[19,20,62] Mg doped *h*-BN epilayers exhibited a p-type conductivity that is several orders of magnitude higher than that of Mg doped AlN. The p-type conductivity type of Mg doped *h*-BN was verified by Hall effect and Seebeck coefficient (or "hot probe") measurements.[19]

We have previously determined the acceptor energy levels of Mg (~0.5 eV) and Zn (~0.6 eV) in AlN.[63-68] The Mg acceptor level (E_A) in $Al_xGa_{1-x}N$ increases with x, from about 170 meV in GaN (x = 0 with E_g ~3.4 eV) to 510 meV in AlN (x = 1 with E_g ~ 6.1 eV),[19,20,63–66] as illustrated in Fig. 9. The free hole concentration (*p*) decreases with the acceptor activation energy following $p \sim \exp(-E_A/kT)$. As a result, the free hole concentration decreases exponentially with a decrease in emission wavelength (or increase in bandgap). An E_A value around 500 meV in AlN translates to only 1 free hole for roughly every 2 billion (2×10^9)incorporated Mg impurities at room temperature. This leads to extremely resistive AlN "p-layers". For instance, an optimized Mg doped AlN epilayer has a typical "p-type resistivity" of $>10^7$ Ω·cm at 300 K.[63,64] This causes an extremely low free hole injection efficiency into the AlGaN quantum well active region and is a major obstacle for the realization of AlGaN-based DUV light emitting devices with high quantum efficiency. It should be noted that

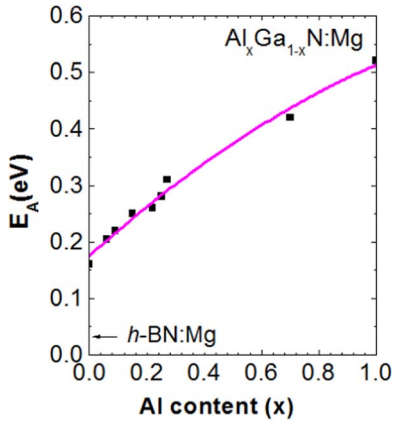

Figure 9. Mg acceptor level (E_A) in AlGaN and *h*-BN. The arrow indicates the measured E_A value in Mg doped hBN epilayers grown by MOCVD (after Ref. 19).

the deepening of the Mg acceptor level in $Al_xGa_{1-x}N$ with increasing x is a fundamental physics problem.

One of the most significant differences between these two materials is the lower acceptor energy level in *h*-BN than in w-AlN. The measured Mg activation energy value in MOCVD grown *h*-BN epilayers appears to be around 31 meV in *h*-BN[19] and is marked in Fig. 9. With optimization in post-growth annealing processes, we were able to obtain a p-type resistivity around 2 Ω·cm at 300 K,[62] which is 6 orders of magnitude reduction compared to those of Mg doped AlN. These preliminary results indicate that *h*-BN has the potential to extend p-type III-nitride materials all the way up to 6 eV. If the wide bandgap and highly conductive *h*-BN p-type layer can be successfully implemented in nitride DUV LEDs, p-type conductivity of the electron blocking and p-contact layers will be dramatically increased. This will significantly improve the free hole injection and quantum efficiency and DUV transparency, reduce the operating voltage and heat generation, and increase the device operating lifetime

To realize devices which require both p-type and n-type *h*-BN materials, n-type conductivity control in *h*-BN is equally important. However, studies on n-type conductivity control have been limited for *h*-BN either in bulk or epilayer form. It seems that Si would be a natural choice as an n-type dopants, which has been established for GaN and AlN. We have investigated the suitability of Si as an n-type dopant in *h*-BN.[69] However, we have shown that in-situ doping of *h*-BN with Si provides n-type conductivity only at high temperatures (above 700 K). As illustrated in Fig. 10, Hall effect measurements

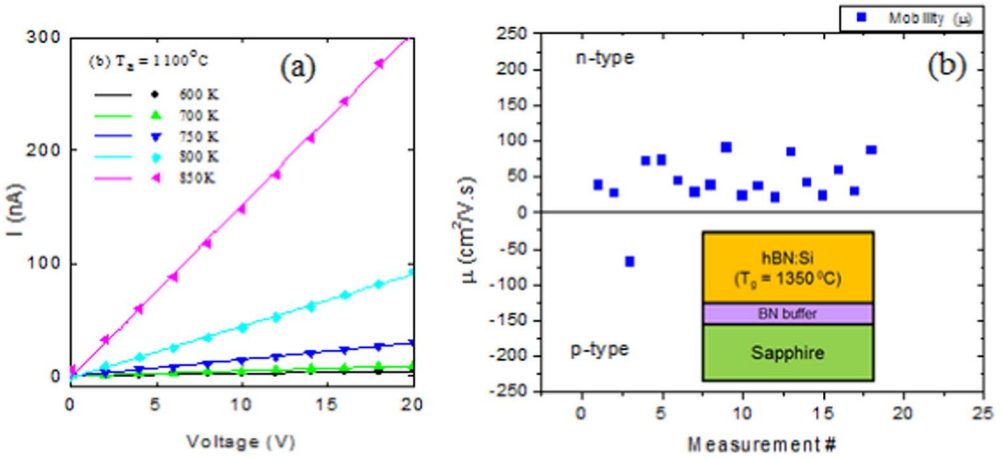

Figure 10. (a) I-V characteristics of an *h*-BN:Si sample grown by MOCVD with silane flow rate of 150 sccm, thermally annealed at a temperature of $T_a = 1100°C$ after growth, measured at different temperatures. (b) Mobility data obtained by Hall effect measurements carried out at 850 K for the same *h*-BN:Si sample. In our experimental setup, +μ means electron conduction and -μ means hole conduction (after Ref. 69).

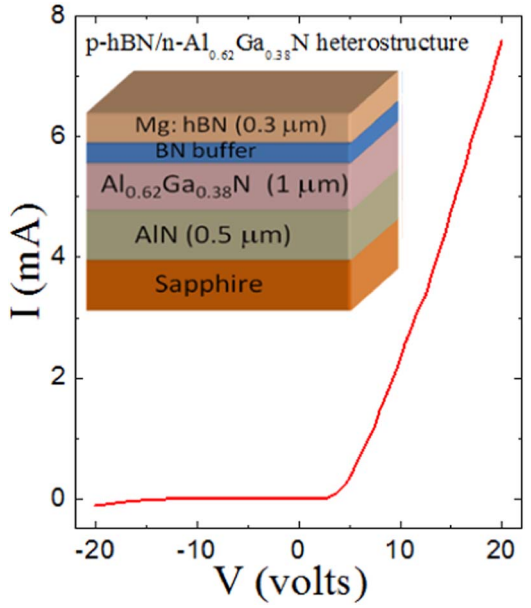

Figure 11. I-V characteristics and schematic illustration of a p-BN:Mg/n-$Al_{0.62}Ga_{0.38}N$/AlN p-n structure in which the buffer layer was doped with Mg and p-contacts were annealed at 1020°C exhibiting a diode behavior (after Ref. 62).

were carried out at 850 K for the sample annealed at $T_a = 1100$°C and yielded an average resistivity $\rho \sim 12\ \Omega \cdot$cm with a free electron density $n \sim 1 \times 10^{16}$ cm^{-3} and mobility $\mu \sim 48$ (± 24) cm^2/V·s. The mobility data unambiguously confirmed that *h*-BN:Si exhibits n-type conductivity. A more recent study carried out for Si doped *h*-BN thin films via ion implantation has shown that it is possible to achieve n-type conduction with a resistivity as low as 0.5 Ω·cm at room temperature and Si doping induces two shallow donor levels in the *h*-BN.[70] Further works are required to understand the mechanisms of conductivity control as well as the choice of dopant species and optimized conditions of post-growth processes of materials, type of metal contacts, and contact annealing conditions.

Hexagonal BN Heterostructures

In order to utilize p-type *h*-BN for AlGaN DUV device applications, the feasibility for producing *h*-BN/AlGaN heterostructures must be investigated. The growth of p-*h*-BN on n-$Al_xGa_{1-x}N$ ($x \sim 0.62$) heterostructures has been attempted.[62] Prior to the n-AlGaN epilayer growth, a 0.5 μm undoped AlN epilayer was first deposited on sapphire substrate to serve as a template and dislocation filter. Si doped n-AlGaN ($x \sim 0.62$) epilayer of about 1 μm thickness exhibits an n-type resistivity of about 0.01 Ω cm. A low temperature BN buffer layer grown at 800°C is incorporated before the growth of *h*-BN epilayer to enhance the adhesion of p-*h*-BN on top of n-$Al_xGa_{1-x}N$. In addition to the need of thermal annealing treatment of the p-contacts, we also found that doping the buffer layer with Mg significantly improves the vertical transport properties. Figure 11 shows the I-V characteristics and schematic illustration of a p-*h*-BN/n-$Al_xGa_{1-x}N$ ($x \sim 0.62$) structure in which the buffer layer was doped with Mg and p-contacts were annealed at 1020°C.[62] The p-*h*-BN/n-$Al_xGa_{1-x}N$ ($x \sim 0.62$) structure exhibits a decent diode behavior. The leakage current under reverse bias can be controlled to be quite low (~3 μA at −10 V). However, DUV light emission under current injection has not yet been achieved. We believe that key parameters to be further optimized include the deposition and p-type doping conditions and thickness of the low temperature buffer layer. More recent work conducted on BN growth on SiC substrate indicated that the use of buffer layer may be not necessary.[71,72] Therefore, it may also be possible to eliminate the buffer layer in the p-*h*-BN/n-$Al_xGa_{1-x}N$ heterojunction.

The current-voltage (I-V) characteristics of the *h*-BN/6*H*-SiC heterostructure were measured and the results were utilized to determine the band offsets of the *h*-BN/6*H*-SiC heterojunctions.[71] The analysis yielded the conduction and valence band offsets (ΔE_C and ΔE_V) of the *h*-BN/6*H*-SiC heterointerface of about 2.3 and 0.7 (±0.2) eV, respectively, giving a $\Delta E_C/\Delta E_g$ value of around 76%. The measured band offsets are in reasonable agreement with values deduced from the band alignments between *h*-BN, AlN, and 6*H*-SiC obtained from independent experimental data and theoretical calculations.

Device Demonstration

The isotope ^{10}B has a very large capture cross section for thermal neutrons of 3840 barns.[73–75] This together with its wide bandgap property makes ^{10}B enriched *h*-BN (*h*-^{10}BN) semiconductor an excellent neutron detector material. The neutron and ^{10}B nuclear reaction is described by the following equations:

$$^{10}B + {}^{1}{}_{0}n \rightarrow {}^{7}Li\,(1.015\ MeV) + \alpha\,(1.777 MeV) \qquad 6\% \qquad [3a]$$

$$^{10}B + {}^{1}{}_{0}n \rightarrow {}^{7}Li^{*}\,(0.840\ MeV) + \alpha^{*}\,(1.470\ MeV)\,. \qquad 94\% \qquad [3b]$$

The daughter particles (α particles and ^{7}Li ions) produced by the nuclear reaction have a mean free path of ~5 μm for α particles and ~2 μm for ^{7}Li ions and lose their energies by producing a cloud of electron-hole pairs in *h*-BN semiconductor, which serve as the detection signal for thermal neutrons. In *h*-BN neutron detectors, the neutron capture, charge collection, and electrical signal generation occur in the same *h*-BN layer, leading to exceptional detection capabilities including high detection efficiency and energy resolution.

We have explored *h*-BN for solid-state thermal neutron detector applications.[76–80] Mobility-lifetime ($\mu\tau$) products of electrons and holes of *h*-BN epilayers were characterized and the results indicate that these MOCVD grown *h*-BN epilayers are suitable for detector fabrication.[76–80] Both lateral metal-semiconductor-metal (MSM) detectors[76–79] and simple vertical "photoconductive-type"[80] of detectors were fabricated. Figure 12a and the inset of Fig. 12b show that the fabricated detectors exhibit very low leakage current density (as low as 10^{-11} A/cm^2) at a bias voltage of 10 V.[24,76–79] As shown in Fig. 12b, as deep UV photodetectors, these devices exhibit a peak responsivity at 217 nm and a cutoff wavelength at around 230 nm with virtually no responses for $\lambda > 230$ nm.[24] The dielectric strength of *h*-BN epilayers exceeds that of AlN epilayers and is greater than 4.4 MV/cm based on the measured result for an *h*-BN epilayer released from the host sapphire substrate.[24] Thus, *h*-BN is a material with a very low dielectric constant, but having a very high dielectric strength. These properties are important for detector applications.

The fabricated *h*-BN detectors were employed for thermal neutron detection and the measured pulse-height spectra shown in Fig. 13 exhibit distinguishable peaks due to the detection of the four product energies expected from the ^{10}B and neutron reaction described by Eq. 3.[77,78] Furthermore, *h*-BN detectors exhibit very high γ-photon rejection.[77] ^{10}B has a cross-section (σ) of 3840 barns (3.84×10^{-21} cm^2) for thermal neutrons (25 meV energy). The density of boron in *h*-BN is 5.5×10^{22} cm^{-3}. Thermal neutrons therefore have an absorption coefficient of $\alpha = N\sigma = 5.5 \times 10^{22} \times 3.84 \times 10^{-21} = 211.2$ cm^{-1} in 100% ^{10}B enriched *h*-BN films. Hence, the absorption length (λ) of thermal neutrons in *h*-^{10}BN can be obtained as $\lambda = 1/\alpha = 1/211.2cm = 4.73 \times 10^{-3}$ cm = 47.3 μm. This means that the attainment of thick layers of *h*-BN is necessary in order to realize *h*-BN detectors with high detection efficiencies. Most recetly, we have successfully realized freestanding 4-inch diameter ^{10}B enriched *h*-BN wafers 43 μm in thickness from epitaxy growth and subsequent mechanical separation from sapphire substrates. A simple vertical "photoconductor-type" detector was fabricated by depositing ohmic contacts on the bottom and top surfaces. The pulse height and efficiency measurements have demonstrated that 43 μm *h*-^{10}BN detectors deliver a detection efficiency of 51.4% for thermal neutrons and a charge collection efficiency of 86.1% at a bias voltage

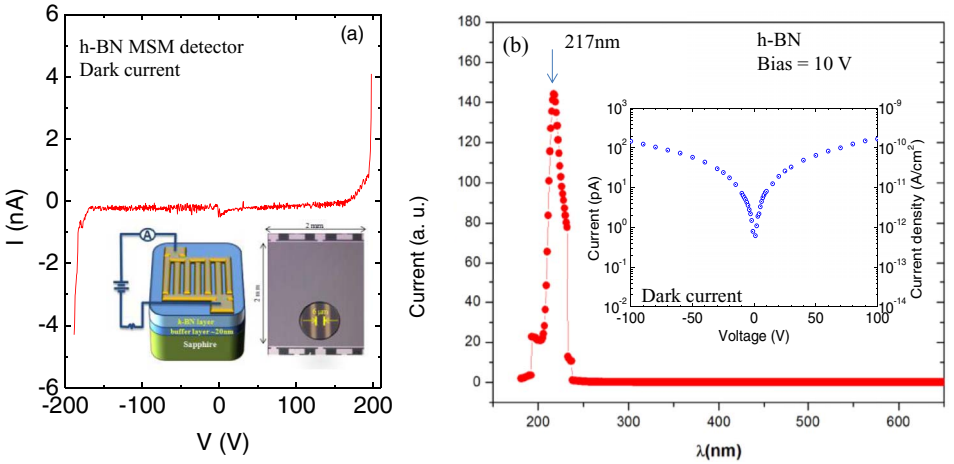

Figure 12. (a) Dark I-V characteristic (leakage current density vs. applied bias voltage) of an *h*-BN MSM detector. The inset are a schematic and an optical image of a fabricated *h*-BN MSM detector (b) The relative photo-spectral response of an *h*-BN MSM photodetector measured at a bias voltage of 10 V. The inset is the dark I-V characteristic in an expanded scale for a clear presentation (after Ref. 24).

of 400 V.[80] This detection efficiency is the highest reported for any semiconductor-based neutron detector. With further developments in material growth and device design, *h*-BN semiconductor detectors with neutron detection sensitivity greatly exceeding those of the current state-of-the-art are anticipated. The ability of producing wafer scale *h*-BN semiconductor materials by techniques such as MOCVD and the applicability of semiconductor processing technologies also open up the possibility to construct sophisticated neutron detectors with high sensitivity at relatively low costs.

Summary

Significant progress in MOCVD growth of *h*-BN epilayers has been made. These MOCVD grown epilayers exhibit highly efficient band-edge photoluminescence (PL) emission lines centered at around 5.5 eV at room temperature. It was observed that the emission of *h*-BN is more than two orders of magnitude higher than that of high quality AlN epilayers. It was shown that the unique 2D structure of *h*-BN induces high density of state (DOS) near the band-edge, which results in high optical absorption (7×10^5/cm vs. $\sim 2 \times 10^5$ /cm for w-AlN) and emission intensity. Polarization-resolved PL results have revealed that *h*-BN is predominantly a surface emission material with light output polarized in the TE mode.

Compared to AlN with a similar energy bandgap, *h*-BN epilayers with p-type conductivity can be obtained. P-type *h*-BN may be used to replace the highly insulating Mg doped AlN in AlGaN based deep UV (DUV) emitters and detectors to enhance the p-type conductivity and reduce the contact resistance. Mg doped *h*-BN epilayers grown on insulating AlN templates exhibit p-type conduction with an in-plane resistivity as low as 2 Ω cm have been obtained through post-growth material and contact annealing processes. Diode behaviors in the p-n structures consisting of p-*h*-BN/n-$Al_xGa_{1-x}N$ (x ∼ 0.62) have been demonstrated. Metal-semiconductors-metal detector structures based on *h*-BN epilayers were fabricated. As deep UV photodetectors, these devices exhibit a peak responsivity at 217 nm and a cutoff wavelength at around 230 nm with virtually no responses for below bandgap excitation. The fabricated *h*-BN detectors exhibit a detection efficiency of 51.4% for thermal neutrons and charge collection efficiency of ∼86%. The dielectric strength of *h*-BN epilayers exceeds that of AlN and is greater than 4.4 MV/cm based on the measured result for an *h*-BN epilayer released from the host sapphire substrate. These results represent a major step toward the realization of *h*-BN based practical devices.

Currently, our understanding of *h*-BN epilayer growth and properties is still in the very early stage compared to the status of AlN epilayers. Much improvement is anticipated for *h*-BN, which ultimately will lead to functional practical devices. However, our results clearly indicate that it is feasible to obtain device quality *h*-BN epilayers by MOCVD growth.

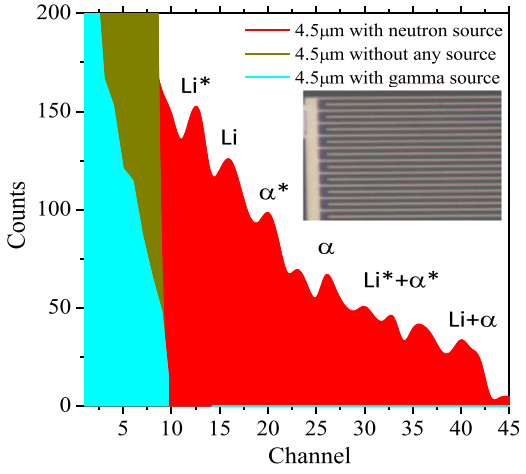

Figure 13. (b) Nuclear reaction pulse height spectrum (counts versus channel number) obtained by a detector incorporating natural *h*-BN of 4.5 μm in thickness with a counting time of 20 minutes. The detector has a dimension of 36 mm^2 (6 mm × 6 mm) and the widths of etched trenches and micro-strips of 10 μm and 10 μm, respectively. The dark yellow and red column bars are the total counts measured in the absence and in the presence of the ^{252}Cf source moderated by a high density polyethylene moderator, respectively. The blue-green column bars represent the measured counts while the detector was irradiated by a γ-photon source produced by ^{137}Cs decay only. The inset is a fabricated *h*-BN MSM detector.

Acknowledgments

The support from the DHS ARI Program (2011-DN-077-ARI048) and the DOE NSSA SSAA program (DE-NA0002927) made research efforts on *h*-BN material growth and neutron detector fabrication possible. The study of the basic structural properties of *h*-BN is supported by the NSF (ECCS-1402886). The authors are grateful to Dr. Jing Li and all the group members in the Center for Nanophotonics at Texas Tech University for their original contributions and to the AT&T Foundation for the support of Ed Whitacre and Linda Whitacre endowed chairs.

References

1. http://www.ioffe.ru/SVA/NSM/Semicond/.
2. S. L. Rumyantsev, M. E. Levinshtein, A. D. Jackson, S. N. Mohammmad, G. L. Harris, M. G. Spencer, and M. S. Shur in *Properties of Advanced SemiconductorMaterials GaN, AlN, InN, BN, SiC, SiGe*, Eds. M. E. Levinshtein, S. L. Rumyantsev, and M. S. Shur, John Wiley & Sons, Inc., New York, 2001, p67.

3. R. W. Lynch and H. G. Drickamer, "Effect of high pressure on the lattice parameters of diamond, graphite, and hexagonal boron nitride," *J. Chem. Phys.*, **44**, 181 (1966).
4. R. S. Pease, "An X-ray study of boron nitride," **5**, 356 (1952).
5. Numerica/Data and Functional/Relationship in *Science and Technology—Crystal and Solid State Physics*, edited by Q. Madelung, Landolt-Bornstein Vol. III, (Springer, Berlin, 1972).
6. Y. Kubota, K. Watanabe, O. Tsuda, and T. Taniguchi, "Deep Ultraviolet Light-Emitting Hexagonal Boron Nitride Synthesized at Atmospheric Pressure," *Science*, **317**, 932 (2007).
7. T. Sugino, K. Tanioka, S. Kawasaki, and J. Shirafuji, "Characterization and field emission of sulfur-doped boron nitride synthesized by plasma-assisted chemical vapor deposition," *Jpn. J. Appl. Phys.*, **36**, L463 (1997).
8. A. Rubio, J. L. Corkill, and M. L. Cohen, "Theory of graphitic boron nitride nanotubes," *Phys. Rev. B*, **49**, 5081 (1994).
9. N. G. Chopra, R. J. Luyken, K. Cherrey, V. H. Crespi, M. L. Cohen, S. G. Louie, and A. Zettl, "Boron-Nitride Nanotubes," *Science*, **269**, 966 (1995).
10. J. Uher, S. Pospisil, V. Linhart, and M. Schiebar, "Efficiency of composite boron nitride neutron detectors in comparison with helium-3 detectors," *Appl. Phys. Lett.*, **90**, 124101 (2007).
11. F. P. Doty, (Sandia National Laboratories), "Boron nitride solid-state neutron detector," US patent, 6727504.
12. N. Alem, R. Erni, C. Kisielowski, M. D. Rossell, W. Gannett, and A. Zettl, "Atomically thin hexagonal boron nitride probed by ultrahigh-resolution transmission electron microscopy," *Phys. Rev. B*, **80**, 155425 (2009).
13. L. Song, L. Ci, H. Lu, P. B. Sorokin, C. Jin, J. Ni, A. G. Kvashnin, D. G. Kvashnin, J. Lou, B. I. Yakobson, and P. M. Ajayan, "Large Scale Growth and Characterization of Atomic Hexagonal Boron Nitride Layers," *Nano Lett*, **10**, 3209 (2010).
14. C. R. Dean, A. F. Young, I. Meric, C. Lee, L. Wang, S. Sorgenfrei, K. Watanabe, T. Taniguchi, P. Kim, K. L. Shepard, and J. Hone, "Boron nitride substrates for high-quality graphene electronics," *Nat. Nanotechnology*, **5**, 722 (2010).
15. L. Britnell, R. V. Gorbachev, R. Jalil, B. D. Belle, F. Schedin, A. Mishchenko, T. Georgiou1, M. I. Katsnelson, L. Eaves, S. V. Morozov, N. M. R. Peres, J. Leist, A. K. Geim, K. S. Novoselov, and L. A. Ponomarenko, "Field-Effect Tunneling Transistor Based on Vertical Graphene Heterostructures," *Science*, **335**, 947 (2012).
16. C. Dean, A. F. Young, L. Wang, I. Meric, G.-H. Lee, K. Watanabe, T. Taniguchi, K. Shepard, P. Kim, and J. Hone, "Graphene based heterostructures," *Solid State Communications*, **152**, 1275 (2012).
17. A. K. Geim and I. V. Grigorieva, "Van der Waals heterostructures," *Nature*, **499**, 419 (2013).
18. K. Watanabe, T. Taniguchi, and H. Kanda, "Direct-bandgap properties and evidence for ultraviolet lasing of hexagonal boron nitride single crystal," *Nat. Materials*, **3**, 404 (2004).
19. R. Dahal, J. Li, S. Majety, B. N. Pantha, X. K. Cao, J. Y. Lin, and H. X. Jiang, "Epitaxially grown semiconducting hexagonal boron nitride as a deep ultraviolet photonic material," *Appl. Phys. Lett.*, **98**, 211110 (2011).
20. H. X. Jiang and J. Y. Lin, "Hexagonal boron nitride for deep ultraviolet photonic devices," *Semicon. Sci. Technol.*, **29**, 084003 (2014).
21. M. Imura, H. Sugimura, N. Okada, M. Iwaya,S. Kamiyama, H. Amano, I. Akasaki, and A. Bandoh, "Impact of high-temperature growth by metal-organic vapor phase epitaxy on microstructure of AlN on 6*H*-SiC substrates," *J. Cryst. Growth*, **310**, 2308 (2008).
22. M. A. Khan, J. N. Kuznia, R. A. Skogman, D. T. Olson, M. M. Millan, and W. J. Choyke, "Low pressure metallorganic chemical vapor deposition of AIN over sapphire substrates," *Appl. Phys. Lett.*, **61**, 2539 (1992).
23. H. J. Kim, S. Choi, D. Yoo, J. H. Ryou, R. D. Dupuis,R. F. Dalmau, P. Lu, and Z. Sitar, "Modulated precursor flow epitaxial growth of AlN layers on native AlN substrates by metal-organic chemical vapor deposition," *Applied Physics Letters*, **93**, 022103 (2008).
24. J. Li, S. Majety, R. Dahal, W. P. Zhao, J. Y. Lin, and H. X. Jiang, "Dielectric strength, optical absorption, and deep ultraviolet detectors of hexagonal boron nitride epilayers," *Appl. Phys. Lett.*, **101**, 171112 (2012).
25. B. N. Pantha, R. Dahal, M. L. Nakarmi, N. Nepal, J. Li, J. Y. Lin, H. X. Jiang, Q. S. Paduano, and D. Weyburne, "Correlation between optoelectronic and structural properties and epilayer thickness of AlN," *Appl. Phys. Lett.*, **90**, 241101 (2007).
26. S. Nakamura, G. Fasol, and S. J. Pearton, "The blue laser diode: the complete story," Springer (2000).
27. Y. Kobayashi, T. Akasaka, and T. Makimoto, "Hexagonal boron nitride grown by MOVPE", *J. Crystal Growth*, **310**, 5048 (2008).
28. B. Arnaud, S. Lebe'gue, P. Rabiller, and M. Alouani, "Huge excitonic effects in layered hexagonal boron nitride," *Phys. Rev. Lett.*, **96**, 026402 (2006).
29. L. Wirtz, A. Marini, and A. Rubio, "Excitons in boron nitride nanotubes: Dimensionality effects," *Phys. Rev. Lett.*, **96**, 126104 (2006).
30. X. K. Cao, B. Clubine, J. H. Edgar, J. Y. Lin, and H. X. Jiang, "Two-dimensional excitons in three-dimensional hexagonal boron nitride," *Appl. Phys. Lett.*, **103**, 191106 (2013).
31. B. Huang, X. K. Cao, H. X. Jiang, J. Y. Lin, and S. H. Wei, "Origin of the significantly enhanced optical transitions in layered boron nitride," *Physical Review B*, **86**, 155202 (2012).
32. S. Majety, X. K. Cao, J. Li, R. Dahal, J. Y. Lin, and H. X. Jiang, "Band-edge transitions in hexagonal boron nitride epilayers," *Appl. Phys. Lett.*, **101**, 051110 (2012).
33. P. B. Perry and R. F. Rutz, "The optical absorption edge of single-crystal AlN prepared by a close-spaced vapor process," *Appl. Phys. Lett.*, **33**, 319 (1978).
34. R. R. Nair, P. Blake, A. N. Grigorenko, K. S. Novoselov, T. J. Booth, T. Stauber, N. M. R. Peres, and A. K. Geim, "Fine Structure Constant Defines Visual Transparency of Graphene", *Science*, **320**, 1308 (2008).
35. K. B. Nam, J. Li, M. L. Nakarmi, J. Y. Lin, and H. X. Jiang, "Deep ultraviolet picosecond time-resolved photoluminescence studies of AlN epilayers," *Appl. Phys. Lett.*, **82**, 1694 (2003).
36. M. Dvorak, S-H Wei, and Z. Wu, "Origin of the variation of exciton binding energy in semiconductors," *Phys. Rev. Lett.*, **110**, 016402 (2013).
37. L. Chen, B. J. Skromme, R. F. Dalmau, R. Schlesser, Z. Chen, C. Sitar, W. Sun, J. Yang, M. A. Khan, M. L. Nakarmi, J. Y. Lin, and H. X. Jiang, "Band-edge exciton states in AlN single crystals and epitaxial layers," *Appl. Phys. Lett.*, **85**, 4334 (2004).
38. K. B. Nam, J. Li, M. L. Nakarmi, J. Y. Lin, and H. X. Jiang, "Unique optical properties of AlGaN alloys and related ultraviolet emitters," *Appl. Phys. Lett.*, **84**, 5264 (2004).
39. J. Li, K. B. Nam, M. L. Nakarmi, J. Y. Lin, H. X. Jiang, Pierre Carrier, and Su-Huai Wei, "Band structure and fundamental optical transitions in wurtzite AlN," *Appl. Phys. Lett.*, **83**, 5163 (2003).
40. T. N. Oder, K. H. Kim, J. Y. Lin, and H. X. Jiang, "III-nitride blue and ultraviolet photonic crystal light emitting diodes," *Appl. Phys. Lett.*, **84**, 466 (2004).
41. H. Kawanishi, M. Senuma, and T. Nukui, *Appl. Phys. Lett.*, **89**, 041126 (2006).
42. K. Watanabe and T. Taniguchi, "Jahn-Teller effect on exciton states in hexagonal boron nitride single crystal", *Phys. Rev. B*, **79**, 193104 (2009).
43. X. Z. Du, J. Li, J. Y. Lin, and H. X. Jiang, "The origin of deep-level impurity transitions in hexagonal boron nitride," *Appl. Phys. Lett.*, **106**, 021110 (2015).
44. X. Z. Du, J. Li, J. Y. Lin, and H. X. Jiang, "The origins of near band-edge transitions in hexagonal boron nitride epilayers," *Appl. Phys. Lett.*, **108**, 052106 (2016).
45. L. Museur and A. Kanaev, "Near band-gap photoluminescence properties of hexagonal boron nitride," *J. Appl. Phys.*, **103**, 103520 (2008).
46. L. Museur, E. Feldbach, and A. Kanaev, "Defect-related photoluminescence of hexagonal boron nitride," *Phys. Rev. B*, **78**, 155204 (2008).
47. J. Wu, Wei-Qiang Han, W. Walukiewicz, J. W. Ager III, W. Shan, E. E. Haller, and A. Zettl, "Raman Spectroscopy and Time-Resolved Photoluminescence of BN and $B_xC_yN_z$ Nanotubes," *Nano Lett.*, **4**, 647 (2004).
48. L. Museur, G. Brasse, A. Pierret, S. Maine, B. Attal-Tretout, F. Ducastelle, A. Loiseau, J. Barjon, K. Watanabe, T. Taniguchi, and A. Kanaev, "Exciton optical transitions in a hexagonal boron nitride single crystal," *Physica Status Solidi (RRL)*, **5**, 214 (2011).
49. M. G. Silly, P. Jaffrennou, J. Barjon, J. S. Lauret, F. Ducastelle, A. Loiseau, E. Obraztsova, B. Attal-Tretout, and E. Rosencher, "Luminescence properties of hexagonal boron nitride: Cathodoluminescence and photoluminescence spectroscopy measurements," *Phys. Rev. B*, **75**, 085205 (2007).
50. P. Jaffrennou, J. Barjon, J.-S. Lauret, B. Attal-Tretout, F. Ducastelle, and A. Loiseau, "Origin of the excitonic recombinations in hexagonal boron nitride by spatially resolved cathodoluminescence spectroscopy," *J. Appl. Phys.*, **102**, 116102 (2007).
51. L. Museur and A. Kanaev, "Near band-gap photoluminescence properties of hexagonal boron nitride," *J. Appl. Phys.*, **103**, 103520 (2008).
52. W. Orellana and H. Chacham, "Stability of native defects in hexagonal and cubic boron nitride," *Phys. Rev. B*, **63**, 125205 (2001).
53. A. Zunger and A. Katzir, "Point defects in hexagonal boron nitride. II. Theoretical studies," *Phys. Rev.*, **11**, 2378 (1975).
54. M. Fanciulli and T. D. Moustakas, "Study of defects in wide bandgap semiconductors by electron paramagnetic resonance," *Physica B*, **185**, 228 (1993).
55. I. Jimenez, A. F. Jankowski, L. J. Terminello, D. G. J. Carlisle, J. A. Sutherland, G. L. Doll, W. M. Tong, D. K. Shuh, and F. J. Himpsel, "Core-level photoabsorption study of defects and metastable bonding configurations in boron nitride," *Phys. Rev. B*, **55**, 12025 (1997).
56. T. B. Ngwenya, A. M. Ukpong, and N. Chetty, "Defect states of complexes involving a vacancy on the boron site in boronitrene," *Phys. Rev. B*, **84**, 245425 (2011).
57. B. Huang and H. Lee, "Defect and impurity properties of hexagonal boron nitride: A first-principles calculation," *Phys. Rev. B*, **86**, 245406 (2012).
58. V. Wang, N. Ma, H. Mizuseki, and Y. Kawazoe, "First-principles study of intrinsic defect properties in hexagonal BN bilayer and monolayer," *Solid State Commun*, **152**, 816 (2012).
59. C. Attaccalite, M. Bockstedte, A. Marini, A. Rubio, and L. Wirtz, "Coupling of excitons and defect states in boron-nitride nanostructures," *Phys. Rev. B*, **83**, 144115 (2011).
60. L. Wirtz, A. Marini, M. Gruning, C. Attaccalite, G. Kresse, and A. Rubio, "Comment on "Huge excitonic effects in layered hexagonal boron nitride" *Phys. Rev. Lett.*, **100**, 189701 (2008).
61. B. Arnaud, S. Lebe'gue, P. Rabiller, and M. Alouani, "Arnaud, Lebègue, Rabiller, and Alouani Reply" *Phys. Rev. Lett.*, **100**, 189702 (2008).
62. S. Majety, J. Li, X. K. Cao, R. Dahal, B. N. Pantha, J. Y. Lin, and H. X. Jiang, "Epitaxial growth and demonstration of hexagonal BN/AlGaN p-n junctions for deep ultraviolet photonics," *Appl. Phys. Lett.*, **100**, 061121 (2012).
63. M. L. Nakarmi, K. H. Kim, M. Khizar, M. Z. Y. Fan, J. Y. Lin, J. Y. , and H. X. Jiang, "Electrical and optical properties of Mg-doped $Al_{0.7}Ga_{0.3}N$ alloys," *Appl. Phys. Lett.*, **86**(9), 092108 (2005).
64. K. B. Nam, M. L. Nakarmi, J. Li, J. Y. Lin, and H. X. Jiang, "Mg acceptor level in AlN probed by deep ultraviolet photoluminescence," *Appl. Phys. Lett.*, **83**, 878 (2003).
65. M. L. Nakarmi, N. Nepal, C. Ugolini, T. M. Al Tahtamouni, J. Y. Lin, and H. X. Jiang, "Correlation between optical and electrical properties of Mg-doped AlN epilayers," *Appl. Phys. Lett.*, **89**, 152120 (2006).
66. M. L. Nakarmi, N. Nepal, J. Y. Lin, and H. X. Jiang, "Photoluminescence studies of impurity transitions in Mg-doped AlGaN alloys," *Appl. Phys. Lett.*, **94**, 091903 (2009).
67. N. Nepal, M. L. Nakarmi, H. U. Jang, J. Y. Lin, and H. X. Jiang, "Growth and photoluminescence studies of Zn-doped AlN epilayers," *Appl. Phys. Lett.*, **89**(19), 192111 (2006).

68. N. Nepal, M. L. Nakarmi, H. U. Jang, J. Y. Lin, and H. X. Jiang, "Growth and photoluminescence studies of Zn-doped AlN epilayers,"*Appl. Phys. Lett.*, **89**, 192111 (2006).
69. S. Majety, T. C. Doan, J. Li, J. Y. Lin, and H. X. Jiang, "Electrical transport properties of Si-doped hexagonal boron nitride epilayers," *AIP Advances*, **3**, 122116 (2013).
70. B. He, M. Qiu, M. F. Yuen, and W. J. Zhang, "Electrical properties and electronic structure of Si-implanted hexagonal boron nitride films," *Appl. Phys. Lett.*, **105**, 012104 (2014).
71. S. Majety, J. Li, W. P. Zhao, B. Huang, S. H. Wei, J. Y. Lin, and H. X. Jiang, "Hexagonal boron nitride and 6*H*-SiC heterostructures," *Appl. Phys. Lett.*, **102**, 213505 (2013).
72. M. Chubarov, H. Pedersen, H. Högberg, Zs. Czigany, and A. Henry, "Chemical vapour deposition of epitaxial rhombohedral BN thin films on SiC substrates," *CrystEngComm*, **16**, 5430 (2014).
73. G. F. Knoll, *Radiation Detection and Measurement*, 3rd ed (J. Wiley, 2000).
74. N. Tsoulfanidis, *Measurement and detection of radiation*, pp. 131, Taylor & Francis, Washington, 1995.
75. O. Osberghaus, "Isotopic abundance of boron. Mass-spectrometric investigation of the electron-impact products of boron trifluoride and boron trichloride," *Zeitschrift fuer Physik*, **128**, 366 (1950).
76. J. Li, R. Dahal, S. Majety, J. Y. Lin, and H. X. Jiang, "Hexagonal boron nitride epitaxial layers as neutron detector materials," *Nucl. Instr. Meth. Phys. Res. A*, **748**, 84 (2014).
77. T. C. Doan, S. Majety, S. Grenadier, J. Li, J. Y. Lin, and H. X. Jiang, "Fabrication and characterization of solid-state thermal neutron detectors based on hexagonal boron nitride epilayers," *Nucl. Instr. Meth. Phys. Res. A*, **748**, 84 (2014).
78. T. C. Doan, S. Majety, S. Grenadier, J. Li, J. Y. Lin, and H. X. Jiang, "Hexagonal boron nitride thin film thermal neutron detectors with high energy resolution of the reaction products," *Nucl. Instr. Meth. Phys. Res. A*, **783**, 121 (2015).
79. T. C. Doan, J. Li, J. Y. Lin, and H. X. Jiang,"Growth and device processing of hexagonal boron nitride epilayers for thermal neutron and deep ultraviolet detectors," *AIP Advances*, to be published.
80. A. Maity, T. C. Doan, J. Li, J. Y. Lin, and H. X. Jiang,"Realization of highly efficient hexagonal boron nitride neutron detectors," *Appl. Phys. Lett.*, **109**, 072701 (2016).